

Supporting Information

The Dual Effect of "Inorganic Fullerene" {Mo₁₃₂} Doped with SnO₂ for Efficient Perovskite-based Photodetectors

Xueying Xu,^a Liming Zhang,^{*b} Ting Wang,^a Yunjiang Li,^a Tuo Ji,^a Weilin Chen,^{*a} Chunlei Wang,^c Chunxia Lin,^d

^a Key Laboratory of Polyoxometalate and Reticular Material Chemistry of Ministry of Education, Faculty of Chemistry, Northeast Normal University, Changchun, 130024, China, E-mail addresses: chenwl@nenu.edu.cn

^b State Key Laboratory of Luminescence and Applications, Changchun Institute of Optics, Fine Mechanics and Physics, Chinese Academy of Sciences, Changchun 130033, China, E-mail addresses: zhangliming@ciomp.ac.cn

^c Library of Northeast Normal University, Changchun, 130024, China

^d Vocational Education Center of Huadian City, Jilin Province, Huadian, 132400, China

The working principle of optoelectronic devices

The photo-generated current of the photodetector and the bias voltage have a significant linear relationship. This indicates that Ohmic contacts are formed when the bias voltage is as high as 3V.¹⁻³ When the perovskite is in contact with the electrode and without additional bias, the device is in equilibrium state, forming a Schottky barrier.⁴ Once a bias voltage is applied to the photodetector device, ion migration and carrier trapping occur at the interface between the perovskite and the electrode, which may cause Ohmic contact on the interface. Under light conditions, the perovskite film generates a large number of photo-generated electrons, which can overcome the semiconductor band gap. The holes introduced by the light pass through the barrier and are then collected by the anode, while the active layer accepts the holes from the anode to realize the photoconductivity of the photodetector.

Supplementary Figures

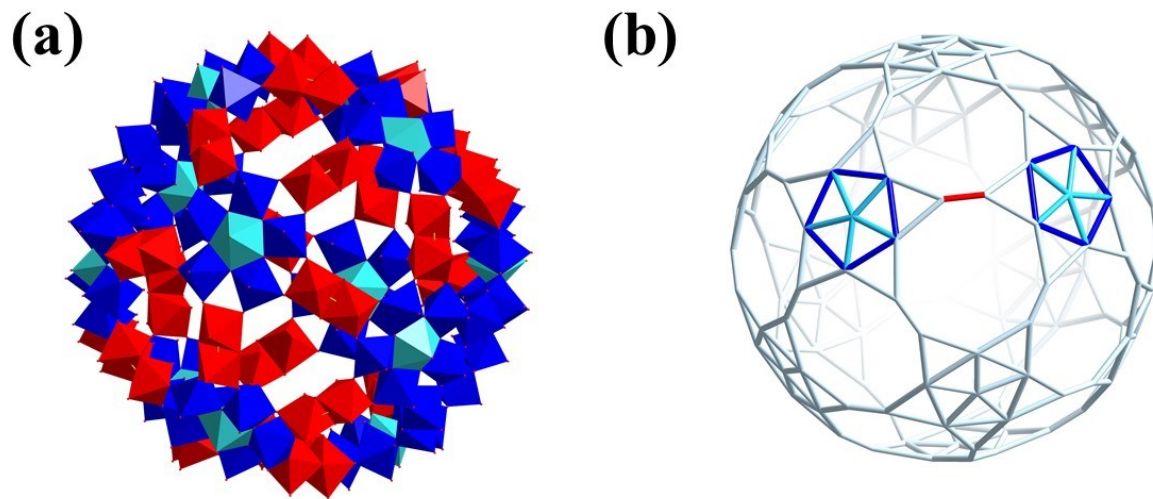


Figure S1. (a) Structural diagram of Mo_{132} ; (b) Schematic representation of the 132 molybdenum atom fragment.

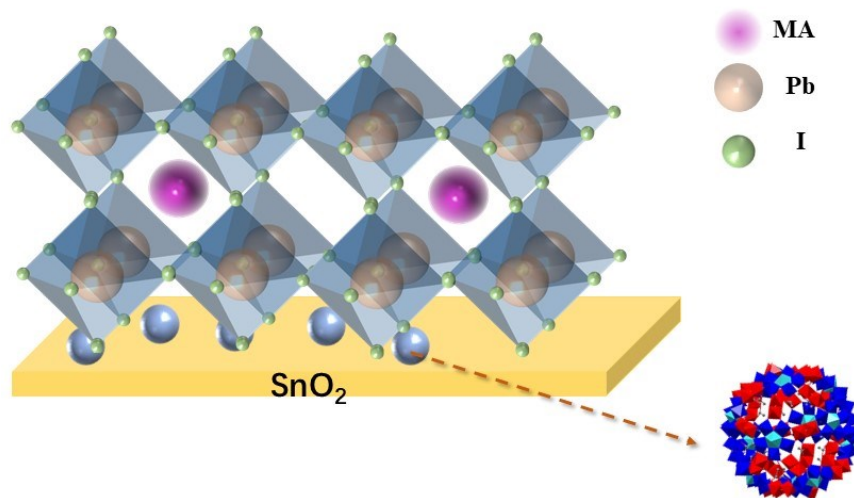


Figure S2. Schematic diagram of Mo_{132} passivation grain boundary

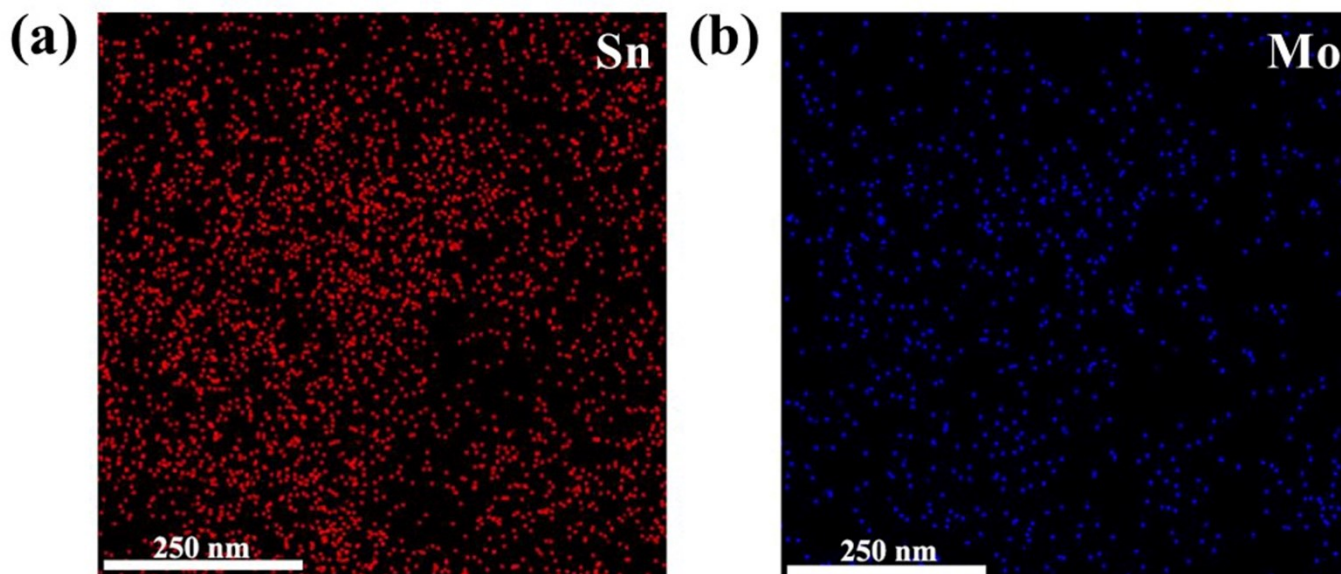


Figure S3. Elemental mappings of Sn and Mo.

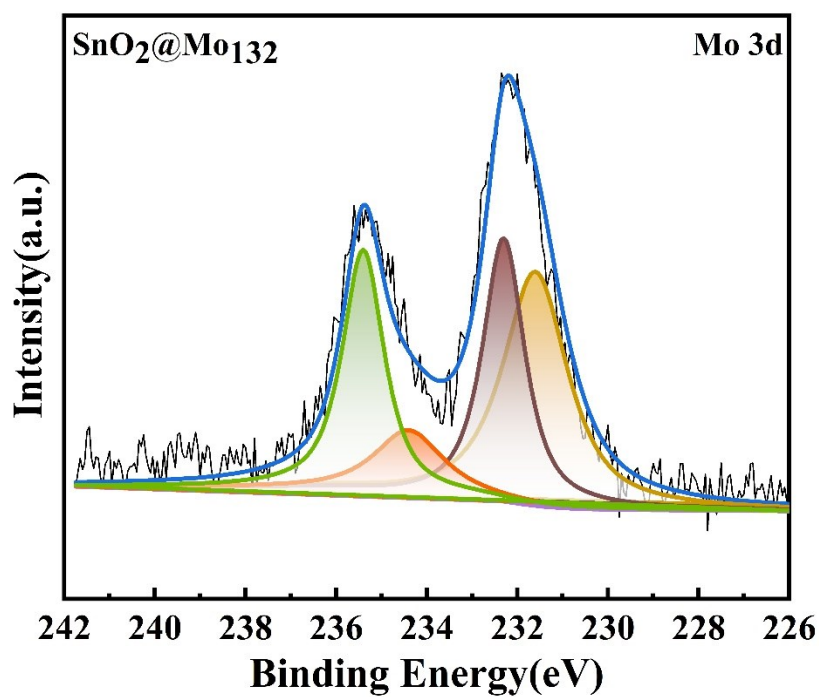


Figure S4. XPS spectrum of SnO₂@Mo₁₃₂ Mo 3d.

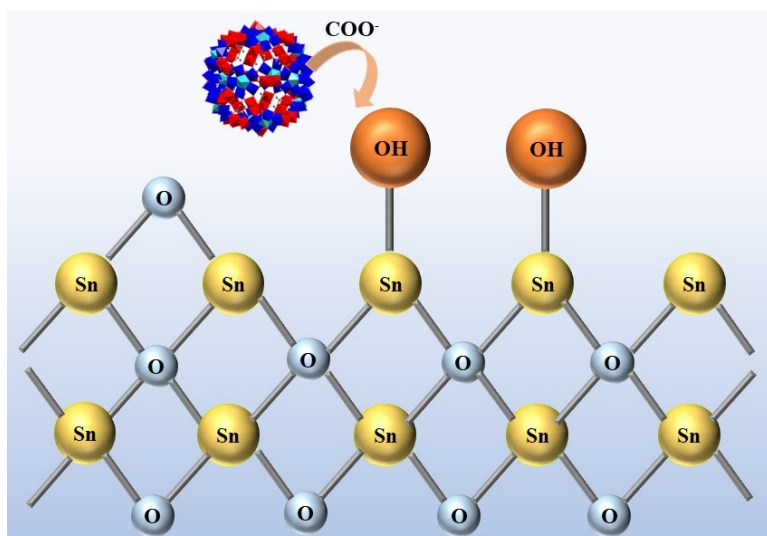
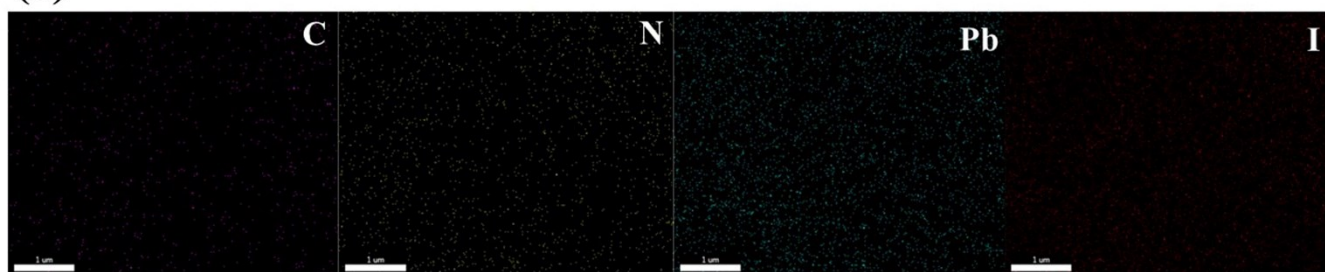


Figure S5. Schematic illustration of doped system of composite.

(a)



(b)

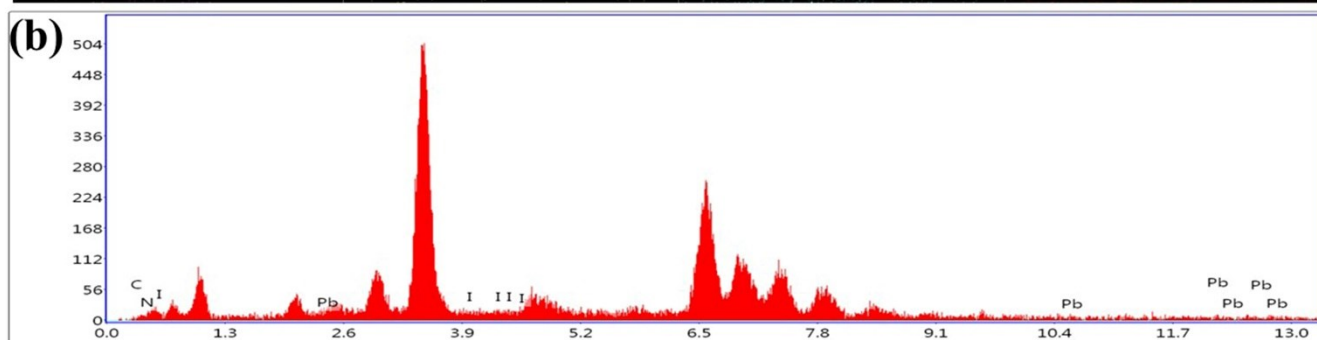


Figure S6. (a) EDS image of $\text{CH}_3\text{NH}_3\text{PbI}_3$, (b) element distribution of four elements

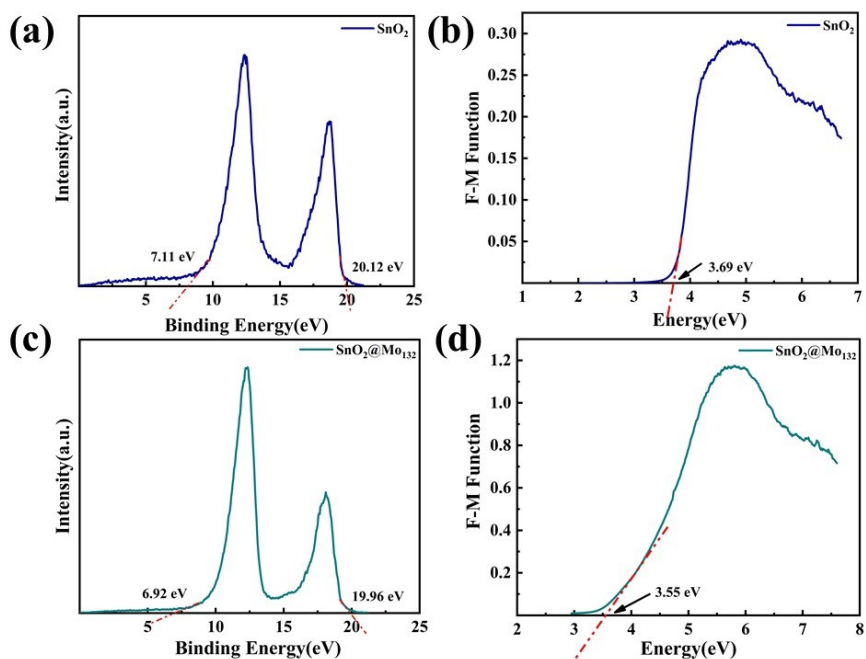


Figure S7. (a) UPS photoemission spectrum of SnO₂; (b) A plot of F against energy E for SnO₂ and the intersection value is the band gap of SnO₂; (c) UPS photoemission spectrum of SnO₂@Mo₁₃₂; (d) A plot of F against energy E for SnO₂@Mo₁₃₂ and the intersection value is the band gap of SnO₂@Mo₁₃₂.

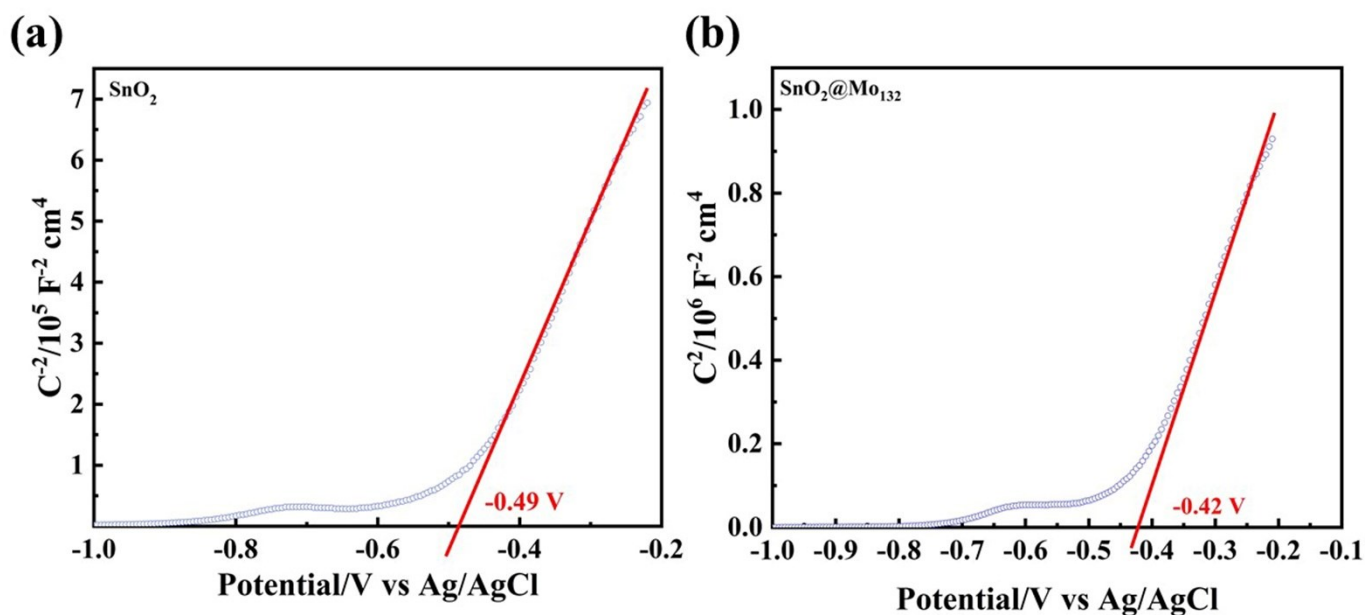


Figure S8. (a) Mott-Schottky curve of SnO₂, (b) Mott-Schottky curve of SnO₂@Mo₁₃₂

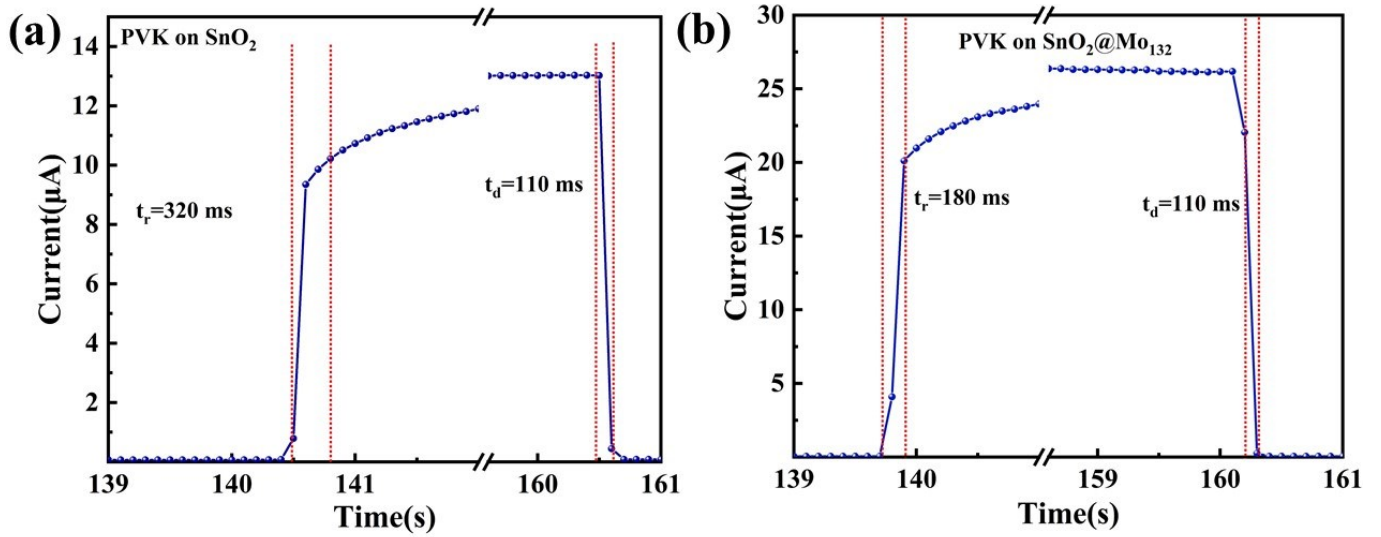


Figure S9. The distensible view of time-dependent photocurrent shows the response time of the reference (a) and modified samples (b) under simulated AM 1.5 illumination.

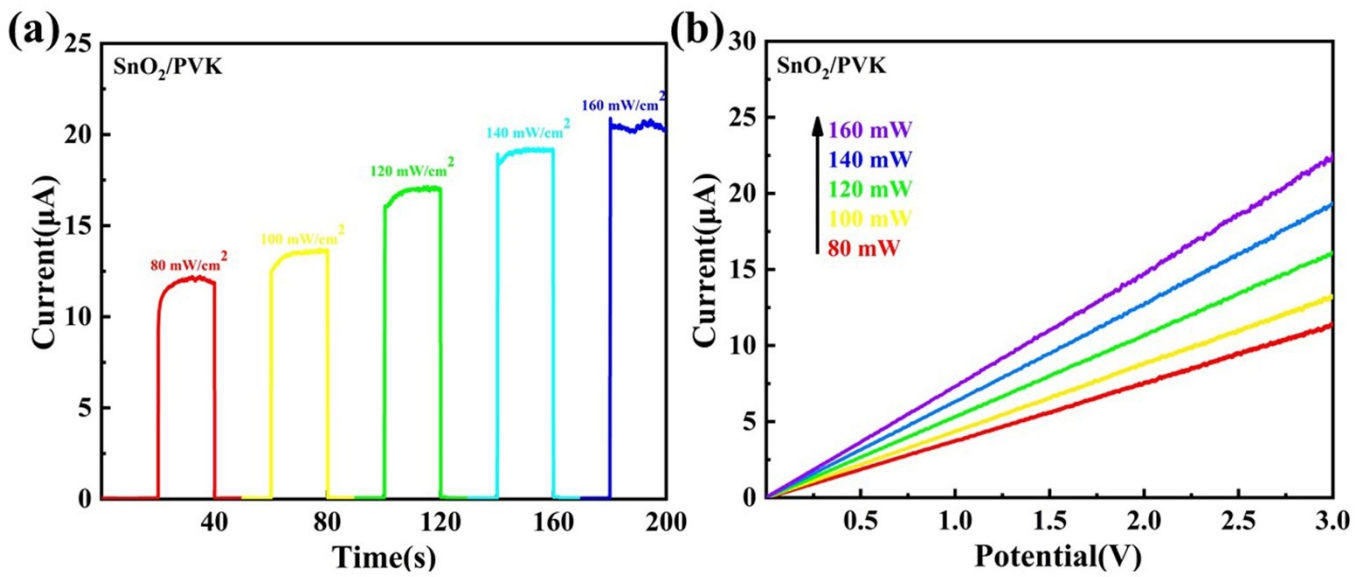


Figure S10. (a) time-resolved current curve of the perovskite-based photodetector on the SnO_2 layer under different light intensities, (b) Corresponding I-V curve.

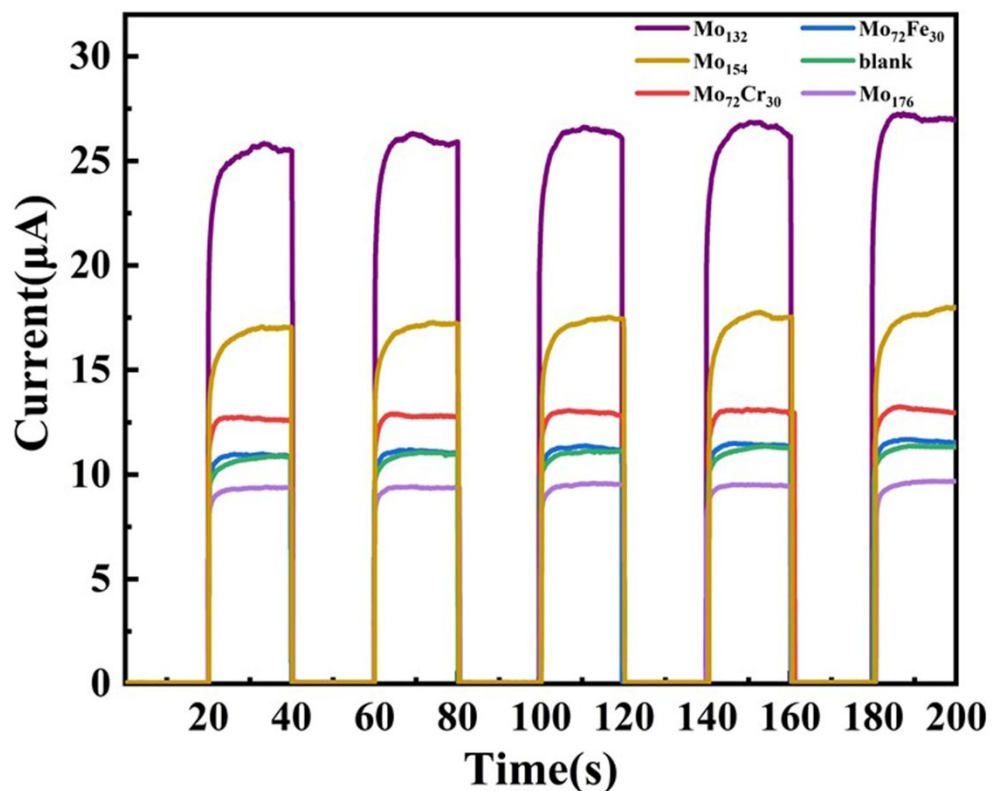


Figure S11. time-resolved current curves of perovskite-based photodetectors with SnO_2 layers doped with different polyoxometalates.

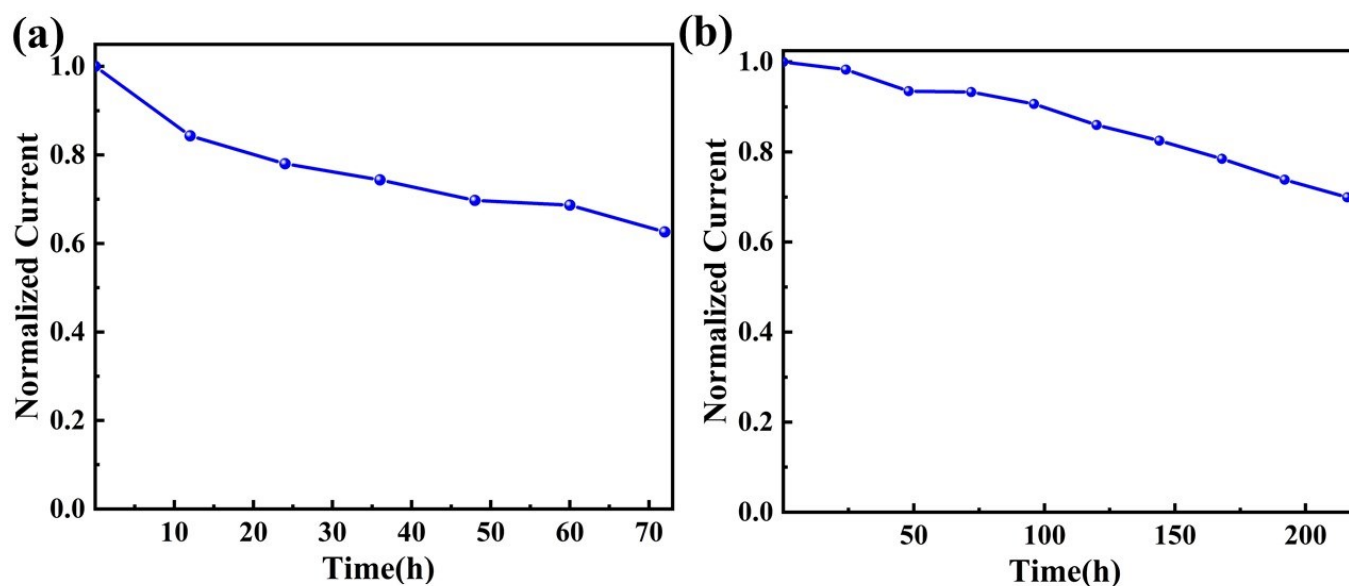


Figure S12. (a) Normalized current values of corresponding devices at 85°C without encapsulation; (b) Normalized current values of corresponding devices in an ambient environment with an RH condition of $45 \pm 5\%$ without encapsulation.

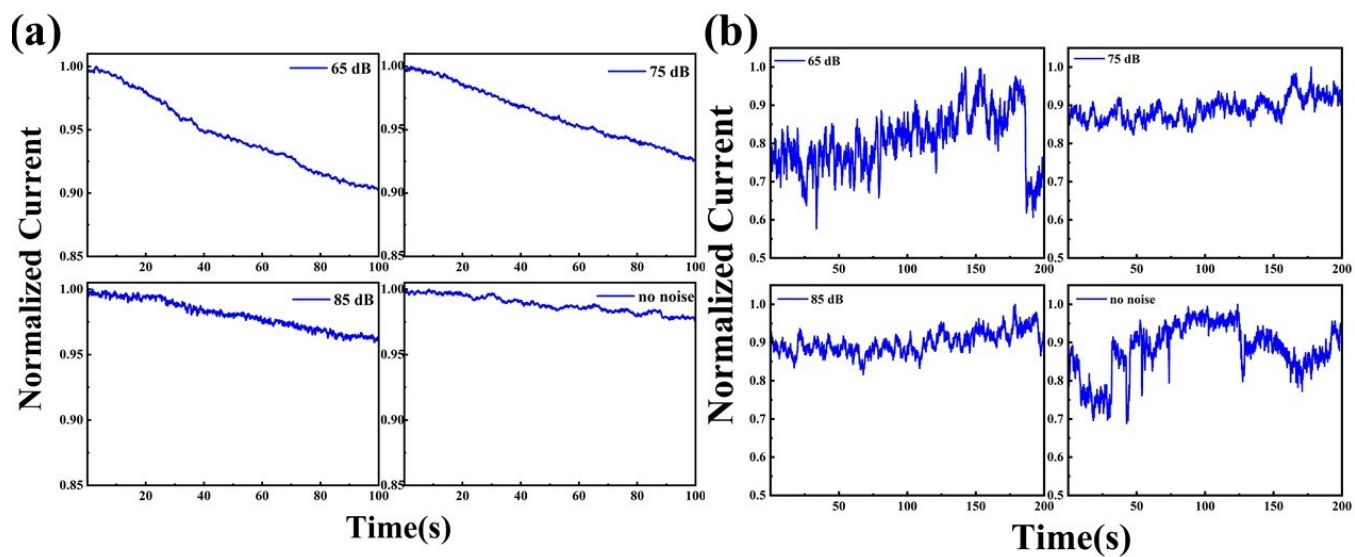


Figure S13. (a) Photocurrent-time curve under different noise conditions under illumination; (b) Photocurrent-time curve under different noise conditions in the dark



Figure S14. Photographs of Mo₁₃₂, SnO₂@Mo₁₃₂ and SnO₂ samples.

Table S1. The area under the deconvoluted subpeaks from the high-resolution O1s spectra of SnO₂ and SnO₂@Mo₁₃₂.

	O ₁	O ₂	O ₃	O _{total}	O _{lattice} (O ₁ /O _{total})	O _{defect} (O ₂ +O ₃ /O _{total})	O _{defect} /O _{lattice}
SnO ₂	39000	21500	2000	62500	0.624	0.376	0.6026
SnO ₂ @Mo ₁₃₂	40000	19000	2000	61000	0.6557	0.3443	0.5251

references

- 1 Y. Liu, F. Li, C. Perumal Veeramalai, W. Chen, T. Guo, C. Wu and T. W. Kim, Inkjet-Printed Photodetector Arrays Based on Hybrid Perovskite CH₃NH₃PbI₃ Microwires, *ACS Appl. Mater. Interfaces*, 2017, **13**, 11662-11668.
- 2 C.-J. Kim, H.-S. Lee, Y.-J. Cho, K. Kang and M.-H. Jo, Diameter-Dependent Internal Gain in Ohmic Ge Nanowire Photodetectors, *Nano Lett.*, 2010, **6**, 2043-2048.
- 3 Lopez-Sanchez, D. Lembke, M. Kayci, A. Radenovic and A. Kis, Ultrasensitive photodetectors based on monolayer MoS₂, *Nat. Nanotechnol.*, 2013, **7**, 497-501.
- 4 F. Zhang, B. Yang, K. Zheng, S. Yang, Y. Li, W. Deng and R. He, Formamidinium Lead Bromide (FAPbBr₃) Perovskite Microcrystals for Sensitive and Fast Photodetectors, *Nano-Micro Lett.*, 2018, **3**, 43.